

Charge-polarized superconducting state emerged in a superatomic antipolar metal

Shuya Xing^{1,4,5,+,*}, Zhongxu Wei^{2,+,*}, Xu Chen^{2,*}, Junming Zhang², Zhenyu Yuan², Jiali Zhao², Feng Jin², Tao Sun², Huifen Ren², Minjie Cui², Hong Chang^{1,4,5}, Tianping Ying², Jiangang Guo², Xiaolong Chen², Shifeng Zhao^{1,4,5}, Wenping Zhou^{1,4,5}, Xinqi Li^{1,4}, Tian Qian², Wei Ji^{3,*}, and Zhihai Cheng^{3,*}

¹*Research Center for Quantum Physics and Technologies, Inner Mongolia University, Hohhot 010021, China*

²*Beijing National Laboratory for Condensed Matter Physics, Institute of Physics, Chinese Academy of Sciences, Beijing 100190, China*

³*Key Laboratory of Quantum State Construction and Manipulation (Ministry of Education), Department of Physics, Renmin University of China, Beijing 100872, China*

⁴*School of Physical Science and Technology, Inner Mongolia University, Hohhot 010021, China*

⁵*Inner Mongolia Key Laboratory of Microscale Physics and Atom Innovation, Inner Mongolia University, Hohhot 010021, China*

Abstract: Symmetry-defined order states play essential roles in determining the emergent exotic physical properties in condensed matter physics, including charge density wave (CDW), polar charge order, and superconducting (SC) states. Recently, the interwoven CDW and antipolar states have been discovered in a low-symmetric superatomic crystal of (Au₆Te₁₂Se₈, ATS), while their delicate interplay with the following emergent SC state at lower temperature remains elusive. Here, we report a real-space experimental investigation on the coexistence and competition of CDW, polar and SC states in the metallic crystal of ATS using scanning tunneling microscopy/spectroscopy combined with transport and Raman measurements. We show that the CDW order is gradually suppressed with the decreased temperature, and a further transformation from antipolar to ferrielectric-like order occurs with the inversion-symmetric broken at the SC state. These spatially observed the emergence and competition of the above ordered states coincide with the temperature-dependent transport and Raman measurements. We predict that the delicate interplay among these states may contribute exotic “hidden” orders in this superatomic metal, suggesting a unique platform for the exploration of intriguing quantum materials.

⁺These authors contributed equally: Shuya Xing and Zhongxu Wei

* Email: 111992026@imu.edu.cn xchen@iphy.ac.cn wji@ruc.edu.cn zhihaicheng@ruc.edu.cn

I. INTRODUCTION

Symmetry-defined orders and their interplay

In low-level quantum materials, there are various symmetry-defined ordered states, which have interdependent or competitive relationships with each other. For instance: in twisted bilayer WSe₂, superconductivity [1, 2], antiferromagnetic (AFM) order [2], and room temperature ferroelectricity [3] emerge at certain specific angles. Vanadium-based kagome lattice materials, AV₃Sb₅ (A = K, Rb or Cs) exhibit superconductivity intertwining with pair density waves [4], chiral CDW [5] as well as the chiral flux phase [6, 7], especially the latter two are states related to inversion symmetry breaking (TRS) or rotational symmetry breaking. In typical high-temperature superconductors: copper-based superconductors and iron-based superconductors, superconductivity is often accompanied by complex charge orders [8], the cooper pair density modulation states [9], nematic phases [10], and magnetic ordering [11, 12] *et. al.* However, the inversion symmetry in most of the above systems is still preserved.

Polar metal and polar superconductor

The inversion symmetry broken is crucial for the formation of polar states. From the perspective of classical physics, the existence of polar metal is unpromising as the itinerant electrons in the metal can greatly screen the long-range dipole interactions. However, in 1965, Anderson and Blount proposed the concept of polar metals, pointing out that in some special situations, the shielding effect of the itinerant electrons on ferroelectric polarization is weakened and decoupled from the transverse optical phonon branches [13]. In 2013, more than half a century later, Shi *et al.* first experimentally obtained the polar metal material LiOsO₃ [14]. Subsequently, researchers have discovered another polar metal, WTe₂, whose polar axis can switch with the direction of the external electric field [15]. The coexistence of polar and superconducting states will be more intriguing, which are considered to be incompatible as the excellent conductivity of cooper pairs in superconductors should be able to counteract polarization [16]. Polar superconductors are rare, but there are still exceptions: in diluted-doped SrTiO₃, the heavily screened Coulomb repulsion gives rise to polarized superconducting states [17, 18], and the superconductivity can be mediated by polarization

[17, 18]. The coupled ferroelectricity and superconductivity in bilayer T_d -MoTe₂ provide a candidate for switching from superconducting to normal metallic states through an external electric field [19, 20]. Moreover, polarized superconductivity has been induced via CDW-driven [21], pressure [22], atomic diffusion [23], as well as gating [24].

Superatomic ATS crystal

In the previous work, we investigated an artificially synthesized quasi-two-dimensional superatomic crystal with extremely low symmetry - Au₆Te₁₂Se₈ (ATS), which exhibited plenty of unexpected quantum states. Au₆Te₁₂Se₈ undergoes a BKT phase transition at 2.8K and enters a two-dimensional superconducting state [25]. We have confirmed the sequential-emerged anisotropic triple-cube charge density wave (TCCDW) and polarized metallic states below 120K and 80K via a low-temperature scanning tunneling microscope (LT-STM, 9K) combined with calculations and other experimental measurements [26]. High-pressure measurements on ATS display the competition between superconductivity and TCCDW, as well as the reentrant superconductivity induced by pressure [27]. However, it is still unclear whether the aforementioned exotic quantum states exist below the superconducting transition temperature, and whether superconducting states coexist with polar states.

Here, we experimentally revealed a charge-polarized superconducting state in ATS crystal using an ultra-low-temperature scanning tunneling microscope (ULT-STM, 300mK) together with transport and Raman measurements. At 300mK, we observed an extraordinary inversion symmetry broken inside the triple-cube-period of the TCCDW along the *a*-axis, which led to the antipolar metallic states transforming into a ferrielectric-like polar order at the SC state. In addition, magnetic susceptibility and Raman measurements show anomalous magnetic responses at \sim 50 K, suggesting the presence of more unexpected quantum states in the system. These exotic quantum states, along with superconducting cooper pairing mechanisms in ATS, require further exploration.

II. Results

A. Superatomic crystal structure and physical properties of ATS

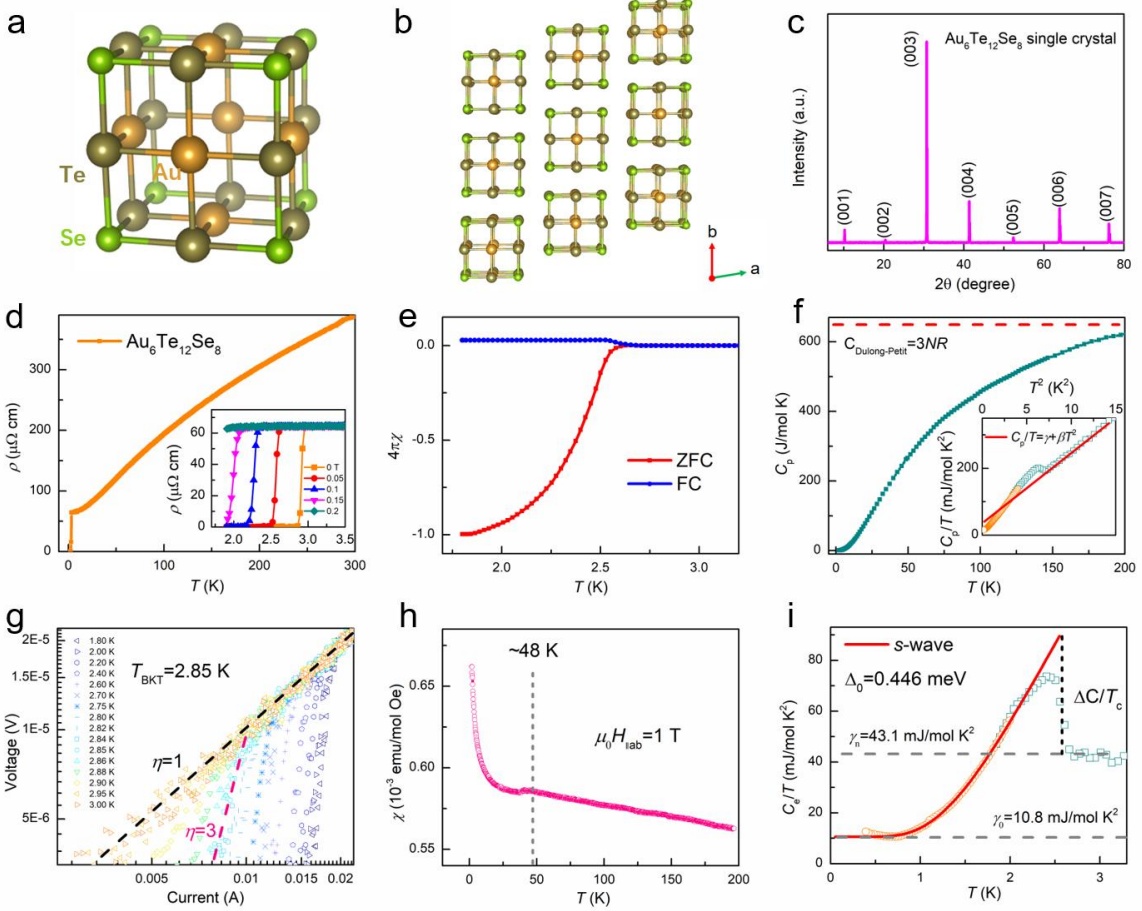


Figure 1. Crystal structure, XRD pattern, and physical properties of $\text{Au}_6\text{Te}_{12}\text{Se}_8$ (ATS). (a) The structure of a single cube of ATS is regarded as a superatom (0D). Au, Te, and Se atoms are represented by golden, brown, and green balls, respectively. (b) 3D crystal structure of ATS in the ab -plane. (c) X-ray diffraction (XRD) pattern of ATS single crystal. (d) Electrical resistivity of ATS from 1.8 to 300 K. The inset shows the electrical resistivity under different magnetic fields. (g) V - I curves of ATS plotted in a log-log scale at various temperatures near T_c . Dash lines denote the fitting result with $V \sim I^\eta$ scaling law, the $\eta = 1$ (black) and 3 (red) curves, respectively. (e) Superconducting volume fractions of ATS under $H = 10 \text{ Oe}$. (h) Temperature dependence of magnetic susceptibility χ and $1/\chi$ of ATS with the magnetic field parallel to the ab plane. (f) Heat capacity (C_p) of ATS as a function of temperature, in which the red dashed line represents the Dulong-Petit limit. The inset shows C_p/T versus T^2 , in which the red straight line represents the fit with the formula $C_p/T = \gamma + \beta T^2$ for the normal-state data. (i) Electronic specific heat divided by temperature C_e/T of ATS in the superconducting state, where $C_e = C - \beta T^3$, and the red line is the theoretical curves calculated as the BCS model.

Figure 1(a)-(b) shows the crystal structure of the superatomic $\text{Au}_6\text{Te}_{12}\text{Se}_8$ (ATS), which consists of rigid cubic blocks with an identical chemical composition of six Au, twelve Te, and eight Se atoms. These cubes are stacked in the ab plane via non-covalent inter-cube quasi-bonds to form a quasi-2D superatomic crystal. Figure 1(c) shows the X-ray diffraction pattern of ATS single crystal. Only (00l) Bragg peaks show up, demonstrating that the largest surface is ab -plane. The peaks are sharp and well-defined, indicating good crystallized quality of the ATS crystal.

Figure 1(d) shows the temperature dependence of the $\rho-T$ curves for the ATS crystal at zero field. The ρ decreases upon cooling, exhibiting a character of good metal. The T_c defined by $\rho = 0$ is near 2.8 K, which is consistent with our previous works. From the bottom inset of Figure 1(d), the low-temperature resistivity of the ATS crystal was measured in magnetic fields up to 0.2 T. With increasing magnetic field, the T_c decreases at the rate of ~ 0.5 K/kOe, confirming the good superconductivity of the sample. Figure 1(g) shows the $V-I$ curves near the critical current at around T_c , in which the critical I_c increases as the temperature decreases and finally reaches 15 mA at 1.8 K. The exponent, η , from power law $V-I^\eta$ increases from 1 (ohmic law) to 3 and more with temperature decreasing. The η reaches 3 at $T_{\text{BKT}} = 2.85$ K, which is the signature of the Berezinskii–Kosterlitz–Thouless (BKT) transition. Figure 1(e) plots the temperature-dependent χ of ATS in zero-field cooling (ZFC) and field-cooling (FC) modes under 10 Oe. The pronounced diamagnetic signals are exhibited below 2.78 K. The superconducting volume fraction is estimated to be 100% at 1.8 K, confirming the bulk superconductivity. Figure 1(h) shows temperature-dependent magnetization measurements performed with the magnetic field perpendicular to the c -axis of ATS crystal under a 1T field. The observed cusp-like anomalies at ~ 48 K coincide with our previous resistivity measurement of the ATS flake sample [25, 26], implying a novel magnetic response, similar to the character in CsV_3Sb_5 and CsCr_3Sb_5 [4, 28, 29].

We measured the specific heat (C_p) of ATS from 0.4 K to 200 K, which is plotted in Figure 1(f). No notable phase transition was observed at 10-200 K, this phenomenon is common in some systems with the CDW-like transition [30, 31]. The inset of Figure 1(f) shows the plot of C_p/T versus T^2 . The SC state of ATS is confirmed by a large

superconducting jump at ~ 2.6 K in the specific heat, coinciding with the electric conductivity and magnetic susceptibility data presented above. In the normal state, the C_p curve is well fitted by $C_p/T = \gamma + \beta T^2$ from 3–10 K, where the first and the second terms correspond to the normal-state electronic and phonon contribution, respectively. Furthermore, we obtain Sommerfeld coefficient $\gamma = 43.1$ mJ mol $^{-1}$ K 2 and $\beta = 20.7$ mJ mol $^{-1}$ K 4 . Extrapolating the data to 0 K leads to a residual $\gamma_0 = 10.8$ mJ mol $^{-1}$ K 2 , indicating a contribution by a non-superconducting phase in volume of about 25%. Thus we obtain the superconducting γ_s as 32.3 mJ mol $^{-1}$ K 2 , which results in the dimensionless jump value of $\Delta C_e/\gamma_s T_c$ of 1.45, see Figure 1(i). This value is consistent with the Bardeen–Cooper–Schrieffer (BCS) value (1.43) for superconductors in the weak coupling limit. The C_e/T data can be fitted by the expression from the BCS theory, $C_e/T \propto e^{-\Delta/k_B T}$. The yielding superconducting gap $\Delta(0) = 0.446$ meV = $5.14 k_B$ K. The good agreement between the measured data and the BCS fitting provides evidence for an *s*-wave isotropic superconducting gap. Furthermore, the fitting yields $2\Delta(0)/k_B T_c = 3.95$, which is a little larger than the value of 3.52 for the BCS weak coupling limit.

B. Electronic states of ATS at 4.6K

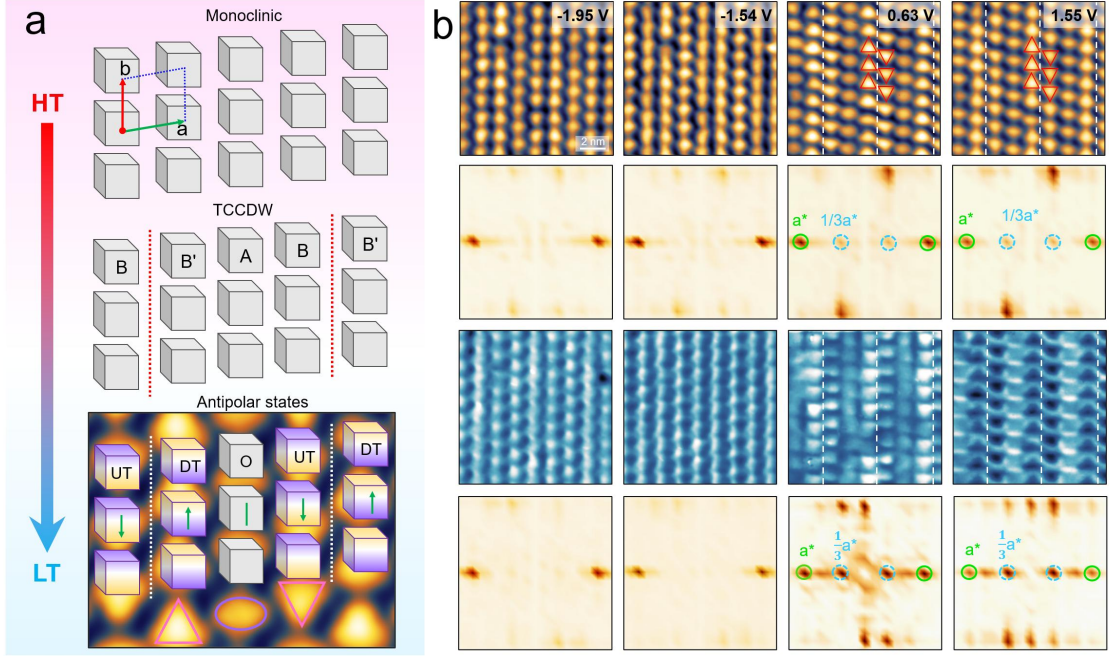


Figure 2. Suppression of TCCDW and antipolar charge orders of ATS crystal at 4.6K (above $T_c=2.8\text{K}$). (a) Schematic of the sequential symmetry-reducing process and emergent ordered states in ATS. (b) STM topography (first row) and corresponding (third row) dI/dV mappings obtained at 4.6K. The second and fourth rows are the corresponding Fast Fourier transform (FFT) patterns. The FFT spots (blue circles) of TCCDW can only be clearly resolved at the empty states with the underlying Bragg spots (green circles) and the marked white lines. The antipolar states are highlighted with the up- and down-triangles in the images of empty states.

Figure 2(a) schematically shows the emergent translation and polar charge orders in the layered ATS super-atomic crystal, which are formed by the sequential symmetry-reducing process of its geometric and electronic structure. The high-symmetric stacking of superatomic building blocks forms a square arrangement. The ATS crystal first undergoes the geometric trimerization of superatomic chains along the a -axis to form the triple-cube CDW (TCCDW) at $\sim 120\text{K}$. The trimerization of cubes breaks the intra-cube inversion symmetry of cube B and B', further resulting in the emergence of intra-cube electronic polarization along the b -axis at $\sim 80\text{K}$. The interweaved TCCDW and antipolar electronic states substantially originate from the low-symmetric geometry structure (P1) of ATS. According to our previous work [26], STM topography performed at 9K shows distinctly “up-triangular” (UT), “olive” (O), and “down-triangular” (DT) shapes in the occupied state, as well as “down-triangular” (UT),

“rhombus” (O), and “up-triangular” (DT) shapes in the unoccupied state, which are manifestations of the two interweaved charge orders in real space.

Figure 2(b) shows the obtained STM topography and corresponding dI/dV mapping at liquid helium temperature (4.6K, above $T_c=2.8$ K). Compared to those at 9K, the tripe-cube-period characteristics of TCCDW get blurry in the STM topography, especially at the occupied states, confirmed by the weak FFT patterns. For the dI/dV mappings, the difference between the occupied and empty states is more definite. In the occupied state, the local density of states (LDOS) exhibits an almost uniform chain-like feature along the b -axis. While in the unoccupied state, the LDOS shows clear TCCDW and antipolar characteristics, highlighted by the white lines and triangles. We can conclude that the preformed TCCDW and antipolar charge orders are suppressed with the temperature decreasing, especially at the occupied states.

C. Electronic states of ATS at 300mK

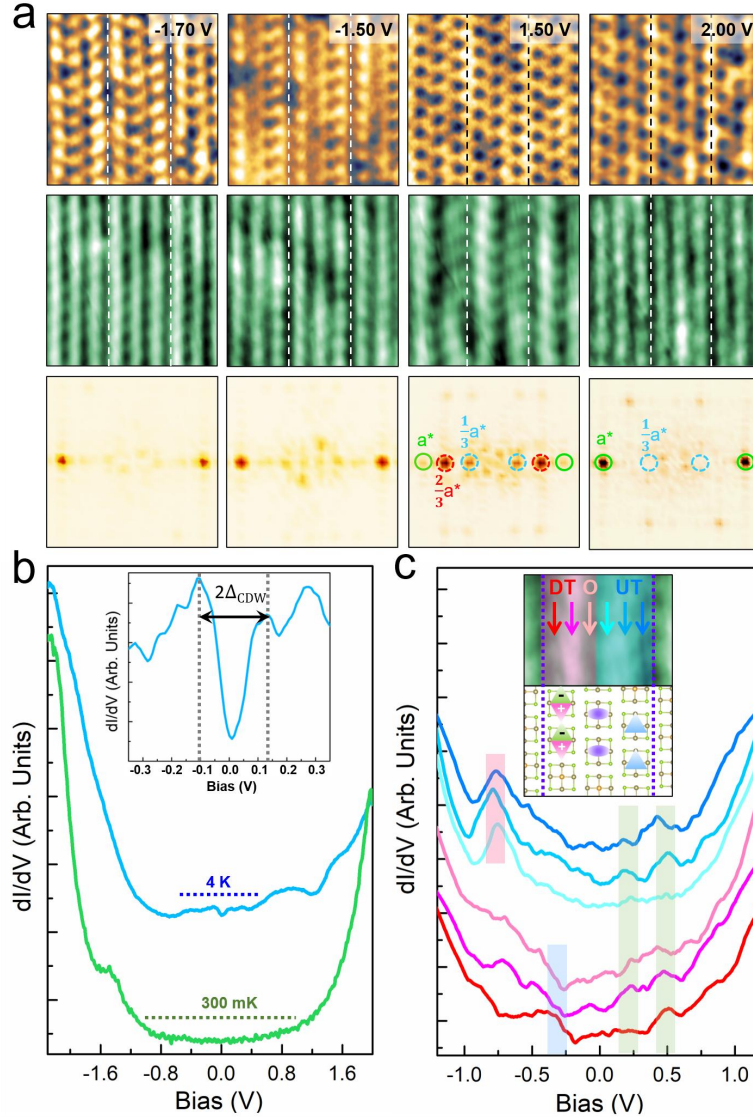


Figure 3. Suppression and modification of the emergent SC state on the preformed TCCDW and antipolar states at 300mK (well below $T_c=2.8\text{K}$). (a) STM topography (first row), dI/dV mapping (second row), and corresponding FFT pattern (third row) of ATS crystal. The characteristics of the triple-cube-period CDW are almost completely suppressed in the dI/dV mappings, while a double-cube-periods appears at 1.5V. (b) STS spectra of ATS crystal at 4.6 K (blue) and 300 mK (green), respectively. The molecular-like gaps increased from ~ 1.2 eV (blue dotted line) to ~ 2.2 eV (green dotted line) with decreased in-gap states. The observed quasigap around the Fermi level is decreased from 0.17 eV (9K) to 0.11eV (4.6K, inset spectra), coincide the suppressed TCCDW state in Fig. 2(a). (c) High-resolution chain-specific STS spectra for the in-gap states at 300 mK, which can be categorized into They were categorized into the left (red-like color) and right (blue-like color) groups, according to the marked in-gap spectra peaks and coincide with the double-cube-period feature of dI/dV mapping at 1.5V.

Figure 3(a) shows the obtained STM topography and corresponding dI/dV mapping at the SC state (300mK, well below $T_c=2.8K$), significantly different from those obtained at 9K and 4.6K. The chain-based TCCDW and antipolar characteristics are difficult to identify at the empty states, and only the tripe-cube-period can be faintly resolved at the occupied states. In the dI/dV mappings, the suppression of SC state on the preformed charge orders is more significant, and neither TCCDW nor antipolar characteristics can be clearly identified even with the eye-guided lines and FFT patterns. It is noted that the double-cube-periods appear in the dI/dV mapping of 1.5V with relative narrow- (left) and wide- (right) chain characteristics. It can be concluded that the preformed TCCDW and antipolar charge orders are greatly suppressed and modified by the emergent SC state at 300mK.

Figure 3(b) shows the dI/dV spectra comparatively obtained at 4.6K (slightly above T_c) and 300mK (greatly below T_c). At the large energy scale, the molecular-like gaps of superatomic cubes were clearly observed and roughly estimated at ~ 1.2 eV (blue line, 4.6K) and ~ 2.2 V (green line, 300mK). The quasigap of TCCDW was decreased from 0.17eV (9K) to 0.11eV (4.6K), as shown by the inset high-resolution spectra of Fig. 3(b). It is also noted that the in-gap spectra weight also significantly decreased from 9K, 4.6K to 300mK. Although the in-gap spectra weight was greatly suppressed at the SC state, there are still several broad and weak spectra peaks that could be resolved. Figure 3(c) shows the obtained chain-specific dI/dV spectra obtained on the triple-cube units at 300 mK. According to the relative weights of broad spectra peaks (-0.75V, -0.3V, 0.3V, and 0.5V), the spectra could be categorized into the left (red-like color) and right (blue-like color) groups, highlighted by the shadows in the inset STM image and STS spectra. The spectra peaks of -0.75V are dominant at the left part, while the other peaks are roughly distributed within the triple-cube units. We can conclude that, in the SC state, not only the pre-formed CDW orders are significantly suppressed, and the inversion symmetry of antipolar order is also further broken in the triple-cube units between the UT (red-like) and DT (blue-like) chains.

D. In-gap ferrielectric-like polar order at the SC state

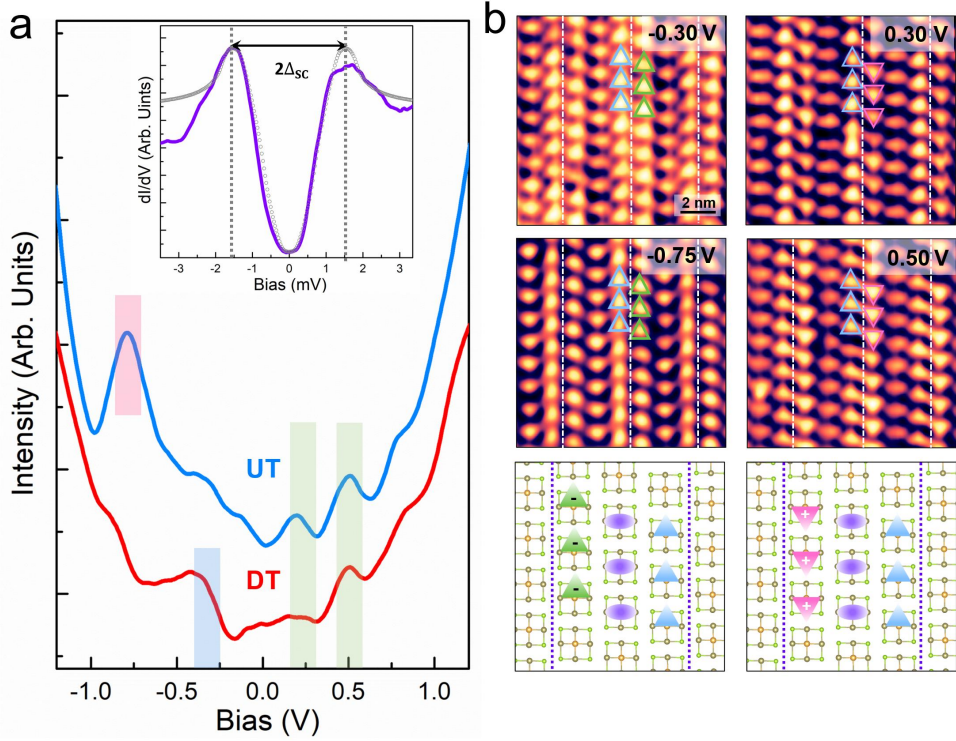


Figure 4. In-gap ferrielectric-like polar order at the SC state. (a) High-resolution STS spectra of the UT (blue) and DT (red) chains with the characteristics in-gap states around -0.75V, -0.3V, 0.3V, and 0.5V. No clear quasigap of TCCDW was observed around the Fermi level, while a "U-shaped" SC gap of ~ 1.5 mV was clearly distinguished at the inset spectra. (b) STM topographies obtained around the in-gap states marked in (a). The triple-cube-period of TCCDW could be readily resolved and marked by the white dashed lines. In the empty states, the inversion-symmetry of UT and DT chains is still preserved and marked by the up- and down-triangles, respectively. While in the occupied states, the inversion-symmetry of UT and DT chains is broken and marked by the up- and up-triangles, respectively. The preserved and broken inversion-symmetry of UT and DT chains is in agreement with the STS spectra of Fig. 4(a). (c) Illustration of in-gap polarized electronic states at filled (left) and empty (right) states. The preformed antipolar order has been converted to a ferrielectric-like polar order by the emergent SC state.

At the SC state, the greatly suppressed CDW order could not contribute a clear quasigap around the Fermi level, as shown in Fig. 4(a), while the weak in-gap spectra peaks can still be roughly distinguished at -0.75V, -0.3V, 0.3V, and 0.5V. The inversion-symmetry broken state between the UT and DT chains is mainly contributed by the occupied states, especially those at the broad peak of ~ 0.75 V. When the energy window is reduced to ± 3 mV, a "U-shaped" SC gap of ATS can be clearly distinguished (inset of Fig. 4(a)). Compared to a single BCS-type isotropic s-wave gap, the coherence peaks exhibited in the SC gap of ATS are not sharp enough [32]. The SC gap size (Δ) is defined as half of the energy spacing between two

coherence peaks and is estimated to be ~ 1.5 meV. According to $\Delta/(k_B \times T_c) \sim 1.76$ is a BCS system, substituting the relevant values: $\Delta = 1.5$ meV and $T_c = 2.8$ K. The calculated result is 6.22, which is much higher than 1.76, indicating that ATS is a super-strong electron correlation system.

The inversion-symmetry broken states are further spatially revealed by the in-gap states of STM images in Figure 4(b). The triple-cube periods of TCCDW still can be readily resolved along the *a*-axis at each spectra peak, while the inversion-symmetric triangular shapes of DT and UT chains are broken along the *b*-axis, as schematically shown in the model of Fig. 4(b). The intra-cube electronic polarization of superatoms shows a triangle-shaped state, resulting from the inversion-symmetry breaking inside the respective DT and UT chain along the *b*-axis. The inversion-symmetric antipolar states from the anti-parallel arrangement of DT and UT chains at 9K are broken in the occupied state at the SC state, while they are still preserved in the unoccupied state. In the occupied state, both UT and DT chains exhibit "up-triangular" shapes, consistent with the observed inversion-symmetry breaking between UT and DT chains within a triple-cube-period CDW in Figure 3(c). The upward-polarization along the DT chains is preserved, indicated by their spatially separated charge accumulation (green triangles, filled states) and charge depletion (red triangles, empty states) distributions in Figure 3(c). While the preformed downward-polarization along the UT chains is annihilated, as shown by their overlapped charge accumulation and depletion distributions (blue triangles, both filled and empty states). The anti-parallel polarization of DT and UT chains interlocked with the TCCDW has been partially eliminated to form a unique polar order at the SC state.

E. Temperature-dependent Raman measurements

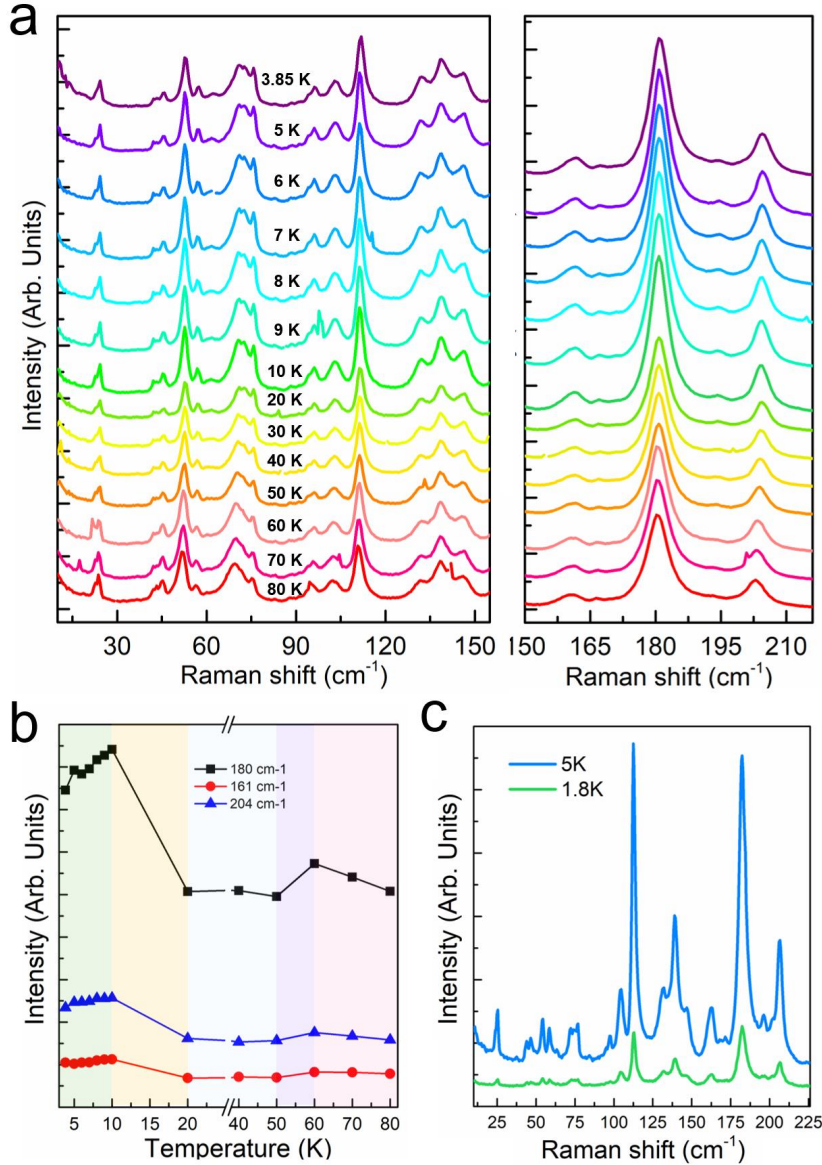


Figure 5. Temperature-dependent Raman spectrum. (a) The temperature-dependent Raman shift of ATS crystal from 80 K to 3.85 K. The left part of the image shows the Raman shift range from 10 cm⁻¹ to 155 cm⁻¹, while the right part shows the range around 180 cm⁻¹. (b) The temperature-dependent intensity of Raman peaks at 161 cm⁻¹, 180 cm⁻¹ and 204 cm⁻¹. The green-shaded area marked the temperature-dependent suppressive effect on Raman intensity below 10K, and a cusp-like anomaly at ~ 50 K (purple-shaded area). (c) Comparison of Raman shifts above (5 K, blue) and below (1.8 K, green) the SC transition temperature ($T_c=2.8$ K). The Raman intensity was greatly suppressed at the SC state.

The step-by-step emergence and evolution of these observed symmetry-defined order states of ATS crystal were further investigated with temperature-dependent Raman measurements based on the above transport and real-space STM measurements. The emergence of TCCDW at ~ 120 K has been previously identified with transport, Raman, and STM measurements, while the following emergence of antipolar charge order at ~ 80 K was mainly identified by the real-space STM measurement. Figure 5(a) shows the obtained temperature-dependent Raman shifts from 80K to 3.85K with six main vibration peaks. As the temperature decreases, the intensity of these six peaks gradually increases from 80 K, followed by a small weakening kink near 50 K (see Supplemental Material for more details). Then, the peak intensity remained unchanged until a sudden increase from 20 K to 10 K. The peak intensity then gradually decreases from 10K to 3.85 K before the superconducting transition. This trend is illustrated by the typical vibration peaks of 180cm^{-1} , 161cm^{-1} , and 204 cm^{-1} shown in Figure 5(b). The emergent SC state significantly suppressed the intensities of Raman peaks at 1.8K compared to those at 5K, as shown in Figure 5(c), consistent with the real-space STM results.

III. Discussion

Symmetry-defined ordering states

As a superatomic metallic material, the unique ATS crystal consists of the step-by-step (1D-2D-3D) stacked high-symmetric molecule cubes (0D, O_h) with the “soft glue” of covalent-like quasi-bonding (CLQB) in an ultra-low-symmetric (triclinic) lattice. The cleaved surface and layers at its *ab*-plane produce the almost lowest symmetry of *P2* (*P211*), while the symmetry-defined order states sequentially emerge through the gradual symmetry-reduced crystal lattice and cube unit. At \sim 120K, a triple-cube CDW (TCCDW) phase occurs through a transverse trimerization process (along the *a*-axis), resulting in the inversion-symmetry broken between the B and B' chains [26]. Then, polarized electronic states (along the *b*-axis) are formed at \sim 80K at the B and B' chains in interlocked antiparallel configuration selectively determined by the preformed TCCDW order.

Spatially polarized metallic states were originally proposed by Anderson and Blount in 1965. Until now, only few of polar metallic materials have been discovered and experimentally confirmed. As the only discovered antipolar metallic state, the SC state is emergent at a lower temperature of 2.8 K within the background of interweaved TCCDW and antipolar charge order. The preformed TCCDW are gradually suppressed from \sim 10K, and the antipolar order is partially and selectively annihilated to form a new ferrielectric-like polar with one polarized and one non-polarized chain. The interlocked inversion-symmetry by the TCCDW is electronically broken due to the difference in intra-cube charge distributions of the polarized and non-polarized chains. It is noted that, in the non-polarized chains, the inversion-symmetry broken is still preserved due to their asymmetric but overlapped charge distributions within the cubes. The temperature-dependent phase diagram of ATS crystal according to the symmetry-defined ordered states is summarized in Fig. S1.

Polar metal to polar superconductor

According to our knowledge, the discovered SC state is the first ferrielectric-like polar state discovered until now, in which the ferrielectric-like polar order is primarily uncovered using real-space STM/STS measurements, and the SC state is verified in both STS and several macroscopic measurements (electrical resistivity, heat captivity, and magnetic

susceptibility). The antipolar metallic state is primarily ascribed to the electronic polarization with the inversion-symmetry broken along the *b*-axis emerging within the high-symmetric cubes rather than the normal spatial displacements of atoms or ions. Due to the gradual suppression of TCCDW from \sim 10K, the interlocked antiparallel polarized configurations are also weakened and are chain-selectively annihilated to a ferrielectric-like polarized configurations with one polar and one non-polar chain at the SC state. The ground state of ATS shows a coexistence and competition of TCCDW, ferrielectric-like polarization, and SC state with complex and delicate interlock and interplay.

Charge-polarized superconducting state

New polar metals and superconductors are being actively discovered and investigated. Here, the ferrielectric-like SC state is discovered in the ultra-low-symmetric superatomic metallic crystal of ATS, which is helpful to independently understand the interplay of different symmetry-defined ordering states. Furthermore, both the anisotropic chain-like structure and high-symmetric large building cubes provide beneficial space to spatially investigate the chain- and cube-specific SC parameters, including the SC gap and phase, with ultra-low-temperature STM. The three chains could show specific-distributed SC parameters due to their different polarized conditions, which are similar but different from the pair density wave (PDW) state discovered in some SC systems. In addition, more detailed and sensitive transport and spectra measurements could be further performed to understand the anisotropic properties of the coexistent ordering state, such as magnetic susceptibility, SHG, ESR, and so on. Finally, given the high tunability of superatomic crystals, including “molecular-like” building blocks, “soft” inter-block interactions, and “engineered” lattice symmetries, the artificial tailoring and construction of exotic quantum states are highly anticipated in the designed superatomic systems.

To summarize, we have discovered an exotic ferrielectric-like charge-polarized superconducting state in a superatomic metallic crystal of ATS, which sequentially undergoes a series of symmetric-broken-defined structural and electronic phase transitions during the temperature decrease. The delicate emergence, interlock, interplay, and competition among these gradually appeared CDW, antipolar, and superconducting ordering states were

phenomenally discussed in this work. More deep and detailed investigation for the ferrielectric-like superconducting state is needed and left for future work.

IV. MATERIALS AND METHODS

Sample preparation

Single crystals of $\text{Au}_6\text{Te}_{12}\text{Se}_8$ (ATS) were grown using the self-flux method, as described in ref [25]. Starting materials with high purity Au powder (99.99%, Sigma Aldrich), Te powder (99.99%, Sigma Aldrich), and Se powder (99.99%, Sigma Aldrich) are stoichiometrically weighted and sealed in an evacuated silica tube in high vacuum and subsequently mounted into a muffle furnace. The furnace was heated up to 850 °C in 24 h and dwelled 48 h. Afterward, the furnace was slowly cooled down to 450 °C in 7 days and then shut down.

STM measurements

STM experiments were performed in a commercial ultrahigh vacuum STM system (USM-1300-³He system with a 16-T magnet) operated in the Synergic Extreme Condition User Facility, Beijing, China. The energy resolution can reach below 0.26 mV. PtIr alloy tips calibrated on clean Ag(111) surfaces were used for all our STM measurements. The STM topography was obtained in the constant-current mode, and the differential conductance (dI/dV) spectra and maps were acquired using a standard lock-in technique at a frequency of 879.9 Hz with modulation voltages of 20 mV and 0.6 mV corresponding to Fig. 3(b), Fig. 3(c), Fig. 4(a), and the inset in Fig. 4(a), respectively. The STM measurements were respectively performed at 4.6K and 300mK to obtain the real space electronic structure above and below the ATS superconducting transition temperature ($T_c \sim 2.8$ K). The STM/STS data were processed using Gwyddion and WSxM software.

XRD, SEM, transport, and Raman measurements

The microstructure of ATS was examined using a scanning electron microscope (SEM, SU5000, HITACHI). The chemical composition of ATS was determined by the Energy Dispersive Spectrum (EDS). Powder X-ray diffraction (PXRD) patterns in the *ab*-plane of single crystal ATS are measured using a Rigaku SmartLab 9kw diffractometer with the Cu-K α anode ($\lambda = 1.5408$ Å). The electrical resistivity (ρ), V-I curves, and specific heat capacity (C_p) of ATS were measured through the standard four-wire method and the thermal relaxation method using the physical property measurement system (PPMS-16, Quantum Design). The specific heat below 1.8 K was measured in the physical property measurement system with a He³ insert. The dc magnetic susceptibility (χ) was characterized using SQUID (MPMS, Quantum Design). The temperature-dependent Raman was measured in the Micro confocal Raman spectrometer (LabRAM HR Evolution, HORIBA) with a continuous-helium-flow optical cryostat.

ACKNOWLEDGMENTS

This project is financially supported by the National Natural Science Foundation of China (Grant Nos. 52302010, 52250308, 92477128), the Ministry of Science and Technology of China, National Key Research and Development Program "Physical Regulation" Special Project (No. 2023YFA1406500), Major research project of China (No. 92477128), Natural Science Foundation of Inner Mongolia Department of Science and Technology Autonomous Region Youth Fund No. 2024QN01010), High level talent introduction and research funding support of Department of Human Resources and Social Security of Inner Mongolia Autonomous Region (No. 12000-150422225). This work was supported by the Synergetic Extreme Condition User Facility (SECUF, <https://cstr.cn/31123.02.SECUF>).

Z.C., S.X., W.J., and X.C. conceived the research project. S.X., Z.W., J.Z., Z.Y., J.Z., and T.Q. performed the STM experiments and analysis of STM data. X.C., T.Y., J.G., X.L.C., and H.C. grew the single crystals. X.C., T.S., H.R., and M.C. performed transport, SEM, and XRD measurements. X.C., S.X., F.J., H.C., and S.Z. performed Raman measurements. X.L., W.Z., and W.J. conducted a theoretical analysis of the experimental data. S.X., X.C., and Z.C. wrote the manuscript with inputs from all authors.

Reference:

[1] Yiyu Xia, Zhongdong Han, Kenji Watanabe, Takashi Taniguchi, Jie Shan and Kin Fai Mak, *Superconductivity in twisted bilayer WSe₂*, *Nature* **637**, 833–838 (2025).

[2] Jinjie Guo, Jordan Pack, Joshua Swann, Luke Holtzman, Matthew Cothrine, Kenji Watanabe, Takashi Taniguchi, David G. Mandrus, Katayun Barmak, James Hone *et al.* Superconductivity in 5.0° twisted bilayer WSe₂, *Nature* **637**, 839–843 (2025).

[3] Yasir Hassan, Budhi Singh, Minwoong Joe, Byoung Min Son, Tien Dat Ngo, Younggeun Jang, Shaili Sett, Arup Singha, Rabindra Biswas, Monika Bhakar *et al.* *Twist-Controlled Ferroelectricity and Emergent Multiferroicity in WSe₂ Bilayers*, *Adv. Mater.* **36**, 2406290 (2024).

[4] Hui Chen, Haitao Yang, Bin Hu, Zhen Zhao, Jie Yuan, Yuqing Xing, Guojian Qian, Zihao Huang, Geng Li, Yuhan Ye *et al.* *Roton pair density wave in a strong-coupling kagome superconductor*, *Nature* **599**, 222–228 (2021).

[5] Chunyu Guo, Carsten Putzke, Sofia Konyzheva, Xiangwei Huang, Martin Gutierrez-Amigo, Ion Errea, Dong Chen, Maia G. Vergniory, Claudia Felser, Mark H. Fischer *et al.* *Switchable chiral transport in charge-ordered kagome metal CsV₃Sb₅*, *Nature* **611**, 461–466 (2022).

[6] Xilin Feng, Kun Jiang, Ziqiang Wang and Jiangping Hua. *Chiral flux phase in the Kagome superconductor AV₃Sb₅*, *Science Bulletin* **66**, 1384–1388 (2021).

[7] M. Michael Denner, Ronny Thomale and Titus Neupert, *Analysis of Charge Order in the Kagome Metal AV₃Sb₅ (A=K; Rb; Cs)*, *Phys. Rev. Lett.* **127**, 217601 (2021).

[8] Changwei Zou, Jaewon Choi, Qizhi Li, Shusen Ye, Chaohui Yin, Mirian Garcia-Fernandez, Stefano Agrestini, Qingzheng Qiu, Xinqiang Cai, Qian Xiao *et al.* *Evolution from a charge-ordered insulator to a high-temperature superconductor in Bi₂Sr₂(Ca, Dy)Cu₂O_{8+δ}*, *Nat. Commun.* **15**, 7739 (2024).

[9] Lingyuan Kong, Michał Papaj, Hyunjin Kim, Yiran Zhang, Eli Baum, Hui Li, Kenji Watanabe, Takashi Taniguchi, Genda Gu, Patrick A. Lee *et al.* *Cooper-pair density modulation state in an iron-based superconductor*, *Nature* **640**, 55–61 (2025).

[10] Anna E. Böhmer, Jiun-Haw Chu, Samuel Lederer and Ming Yi, *Nematicity and nematic fluctuations in iron-based superconductors*, *Nat. Phys.* **18**, 1412–1419 (2022).

[11] Changkai Zhang, Jheng-Wei Li, Dimitra Nikolaidou, and Jan von Delft, *Frustration-Induced Superconductivity in the t-t'Hubbard Model*, *Phys. Rev. Lett.* **134**, 116502 (2025).

[12] Morten H. Christensen, Brian M. Andersen, and Panagiotis Kotetes, *Unravelling incommensurate magnetism and its emergence in iron-based superconductors*, *Phys. Rev. X* **8**, 041022 (2018).

[13] P. D. Anderson and E. I. Blount, *Symmetry considerations on martensitic transformations: "ferroelectric" metals?* *Phys. Rev. Lett.* **14**, 217 (1965).

[14] Youguo Shi, Yanfeng Guo, Xia Wang, Andrew J. Princep, Dmitry Khalyavin, Pascal Manuel, Yuichi Michiue, Akira Sato, Kenji Tsuda, Shan Yu *et al.* *Aferroelectric-like structural transition in a metal*, *Nat. Mater.* **12**, 1024–1027 (2013).

[15] Zaiyao Fei, Wenjin Zhao, tauno A. Palomaki, Bosong Sun, Moira K. Miller, Zhiying Zhao, Jiaqiang Yan, Xiaodong Xu and David H. Cobden, *Ferroelectric switching of a two-dimensional metal*, *Nature* **560** 336–339 (2018).

[16] Sayantika Bhowal and Nicola A. Spaldin, *Polar metals: principles and prospects*, *Annual Rev. of Mater. Research* **53**, 53–79 (2023).

[17] Pavel A. Volkov, Premala Chandra and Piers Coleman, *Superconductivity from energy fluctuations in dilute quantum critical polar metals*, *Nat. Commun.* **13**, 4599 (2022).

[18] C. Enderlein, J. Ferreira de Oliveira, D. A. Tompsett1, E. Baggio Saitovitch, S. S. Saxena, G. G. Lonzarich and S. E. Rowley, *Superconductivity mediated by polar modes in ferroelectric metals*, *Nat. Commun.* **11**, 4852 (2020).

[19] Apoorv Jindal, Amartyajyoti Saha, Zizhong Li, Takashi Taniguchi, Kenji Watanabe, James C. Hone, Turan Birol, Rafael M. Fernandes, Cory R. Dean, Abhay N. Pasupathy *et al.* *Coupled ferroelectricity and superconductivity in bilayer Ta_xMoTe₂*, *Nature* **613**, 48–52 (2023).

[20] Kenji Yasuda, *Electric switch found for a superconductor*, *Nature* **613**, 33–34 (2023).

[21] Shangfei Wu, Turan Birol, Fei-Ting Huang, Xianghan Xu, Sang-Wook Cheong, Ethan T. Ritz, and Girsh Blumberg, *Polar charge density wave in a superconductor with crystallographic chirality*, *Nat.*

Commun. **15**, 9276 (2024).

[22] Xiaohui Yu, Wei Zhong, Saori Kawaguchi, Hirokazu Kadobayashi, Xiaolin Wang, Zhenxiang Cheng, Changfeng Chen, Binbin Yue, Jian-Tao Wang, Ho-Kwang *et al.* *Coexistence of superconductivity and sliding polar metal state in HgPSe₃*, [arXiv:2410.22823](https://arxiv.org/abs/2410.22823).

[23] Xian-Kui Wei, Abdur Rehman Jalil, Philipp Rüßmann, Yoichi Ando, Detlev Grützmacher, Stefan Blügel, and Joachim Mayer, *Atomic diffusion-induced polarization and superconductivity in topological insulator based heterostructures*, ACS Nano **18**, 571–580 (2024).

[24] Yuki M. Itahashi, Toshiya Ideue, Yu Saito, Sunao Shimizu, Takumi Ouchi, Tsutomu Nojima and Yoshihiro Iwasa, *Nonreciprocal transport in gate-induced polar superconductor SrTiO₃*, Sci. Adv. **6**, eaay9120 (2020).

[25] J.G. Guo, X. Chen, X.Y. Jia, Q.H. Zhang, N. Liu, H.C. Lei, S.Y. Li, L.Gu, S.F. Jin and X.L. Chen, *Quasi-two-dimensional superconductivity from dimerization of atomically ordered AuTe₂Se_{4/3} cubes*, Nat. Commun. **8**, 871 (2017).

[26] Shuya Xing, Linlu Wu, Zilu Wang, Xu Chen, Haining Liu, Shuo Han, Le Lei, Linwei Zhou, Qi Zheng, Li Huang *et al.* *Interweaving Polar Charge Orders in a Layered Metallic Superatomic Crystal*, Phys. Rev. X **12**, 041034 (2022).

[27] Xu Chen, Ge Fei, Yanpeng Song, Tianping Ying, Dajian Huang, Bingying Pan, Dongliang Yang, Xiaofan Yang, Keyu Chen, Xinhui Zhan *et al.* *Superatomic-Charge-Density-Wave in Cluster-Assembled Au₆Te₁₂Se₈ Superconductors*, J. Am. Chem. Soc. **144**, 20915–20922 (2022).

[28] Brenden R. Ortiz, Samuel M. L. Teicher, Yong Hu, Julia L. Zuo, Paul M. Sarte, Emily C. Schueller, A. M. Milinda Abeykoon, Matthew J. Krogstad, Stephan Rosenkranz, Raymond Osborn *et al.* CsV₃Sb₅: A Z₂ topological kagome metal with a superconducting ground state, Phys. Rev. Lett. **125**, 247002 (2020).

[29] Yidian Li, Yi Liu, Xian Du, Siqi Wu, Wenxuan Zhao, Kaiyi Zhai, Yinqi Hu, Senyao Zhang, Houke Chen, Jieyi Liu *et al.* *Electron correlation and incipient flat bands in the Kagome superconductor CsCr₃Sb₅*, Nat. Commun. **16**, 3229 (2025).

[30] Shaohua Liu, Qingchen Duan, Baizhuo Li, Jiaoqiao Meng, Wuzhang Yang, Yi Liu, Yi-Qiang Lin, Si-Qi Wu, Jiayi Lu, Jin-Ke Bao *et al.* *Superconductivity and Charge-Density-Wave-Like Transition in Th₂Cu₄As₅*, J. Am. Chem. Soc. **146**, 8260–8268 (2024).

[31] Xu Chen, Jiangang Guo, Chunsheng Gong, Erjian Cheng, Congcong Le, Ning Liu, Tianping Ying, Qinghua Zhang, Jiangping Hu, Shiyan Li *et al.* *Anomalous Dome-like Superconductivity in RE₂(Cu_{1-x}Ni_x)₅As₃O₂ (RE = La, Pr, Nd)*, iScience **14**, 171–179 (2019).

[32] Ming-Qiang Ren, Shu-Ze Wang, Sha Han, Can-Li Song, Xu-Cun Ma, and Qi-Kun Xue, *Tuning the electronic states and superconductivity in alkali fulleride films*, AAPPS Bull. **32**, 1 (2022).